# Micromechanical properties of biological silica in skeletons of deep-sea sponges

Alexander Woesz
*Max Planck Institute of Colloids and Interfaces, Department of Biomaterials, D-14424 Potsdam, Germany*

James C. Weaver
*Institute for Collaborative Biotechnologies and the Materials Research Laboratory, University of California, Santa Barbara, California 93106-5100*

Murat Kazanci
*Max Planck Institute of Colloids and Interfaces, Department of Biomaterials, D-14424 Potsdam, Germany*

Yannicke Dauphin
*UMR 8148 IDES, Universite Paris XI-Orsay, 91405 Orsay cedex, France*

Joanna Aizenberg
*Bell Laboratories, Lucent Technologies, Murray Hill, New Jersey 07974*

Daniel E. Morse
*Institute for Collaborative Biotechnologies and the Materials Research Laboratory, University of California, Santa Barbara, California 93106-5100*

Peter Fratzl[a)]
*Max Planck Institute of Colloids and Interfaces, Department of Biomaterials, D-14424 Potsdam, Germany*

(Received 15 December 2005; accepted 20 April 2006)

The silica skeleton of the deep-sea sponge *Euplectella aspergillum* was recently shown to be structured over at least six levels of hierarchy with a clear mechanical functionality. In particular, the skeleton is built of laminated spicules that consist of alternating layers of silica and organic material. In the present work, we investigated the micromechanical properties of the composite material in spicules of *Euplectella aspergillum* and the giant anchor spicule of *Monorhaphis chuni*. Organic layers were visualized by backscattered electron imaging in the environmental scanning electron microscope. Raman spectroscopic imaging showed that the organic layers are protein-rich and that there is an OH-enrichment in silica near the central organic filament of the spicule. Small-angle x-ray scattering revealed the presence of nanospheres with a diameter of only 2.8 nm as the basic units of silica. Nanoindentation showed a considerably reduced stiffness of the spicule silica compared to technical quartz glass with different degrees of hydration. Moreover, stiffness and hardness were shown to oscillate as a result of the laminate structure of the spicules. In summary, biogenic silica from deep-sea sponges has reduced stiffness but an architecture providing substantial toughening over that of technical glass, both by structuring at the nanometer and at the micrometer level.

## I. INTRODUCTION

Much is known about the structure and properties of the skeleton of the sponge *Euplectella aspergillum*, but fairly little is known about the biology and ecology of this species. It belongs to the phylum Porifera and is a member of the class Hexactinellida, which includes the predominantly deep-sea glass sponges. Hexactinellids occur in all oceans, especially around the Antarctic continent at depths of 100–1000 m, where they can be up to 90% of the benthic biomass. These unique sponges are among the earliest multicellular animals known from the fossil record, found in rock formations up to 540 million years old.[1,2] Many of the hexactinellids host a wide range

[a)]Address all correspondence to this author.
e-mail: fratzl@mpikg.mpg.de
DOI: 10.1557/JMR.2006.0251

 

of commensal organisms, and *E. aspergillum* is no exception. Within the cylindrical skeleton of this species usually dwells a mated pair of shrimp, which is imprisoned for life. These shrimp are fairly large (~30 mm) and could, if attempting to break free, load the sponge's skeleton with non-negligible forces.[3,4]

The skeleton of *E. aspergillum* (Fig. 1) consists of spicules made from amorphous hydrated silica cemented together by additional silica layers. This complex biomineralized structure was recently found to be structured over at least six levels of hierarchy.[5] At the micrometer scale, there is an arrangement of silica layers around a proteinaceous axial filament.[6–8] The silica layers are a few hundred nanometers up to two micrometers thick and separated by thin organic layers of submicrometer dimensions (Fig. 2).

These thin organic layers, although accounting for not more than a few percent of the overall volume,[9,10] increase the fracture toughness considerably, as one can easily imagine when looking at the fracture surface in Fig. 2.

Another hexactinellid, *Monorhaphis chuni,* has a single anchoring spicule with a diameter of up to 8 mm and a length of 3 m (Fig. 3). This giant spicule is, much like the hair-like anchor spicules of *E. aspergillum*, constructed from silica layers separated from each other by thin layers of organic matter. Compared to the spicules of *E. aspergillum*, the thickness of the silica layers of the giant spicules is much greater; up to 10 μm.

The micromechanical properties of this biogenic silica material are largely unknown and investigated here with nanoindentation on embedded spicule cross sections, in combination with structural characterization using scanning electron microscopy, Raman spectroscopic imaging, and small-angle x-ray scattering (SAXS).

## II. MATERIALS AND METHODS

The anchor spicule of one *Monorhaphis chuni* sponge [collected from western New Caledonia, near Lifou (Loyalty Island) at a depth of 1905 m during the CALSUB campaign in 1989] as well as four specimens of *Euplectella aspergillum* (of Philippine origin) were used in this study. Twelve anchor spicules from a single specimen of *E. aspergillum* were extracted without further treatment for fracture experiments and for SAXS analysis. Additionally, several lattice portions were harvested for etching experiments. Finally, portions of all four *E. aspergillum* specimens as well as the anchor spicule of *M. chuni* and a bundle of anchor spicules of one specimen of *E. aspergillum* were resin embedded for environmental scanning electron microscope (ESEM) and Raman and nanoindentation analysis using procedures described in the following sections.

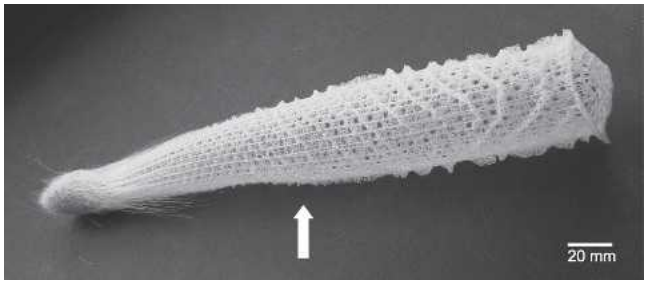


FIG. 1. The skeleton of *Euplectella aspergillum*, from the spicules anchored in the soft sediments of the sea floor (left hand side) to the cap, all made from silica and a very small fraction of organic matter. The arrow indicates the approximate position where the portions of skeletal lattice used for nanoindentation were harvested.

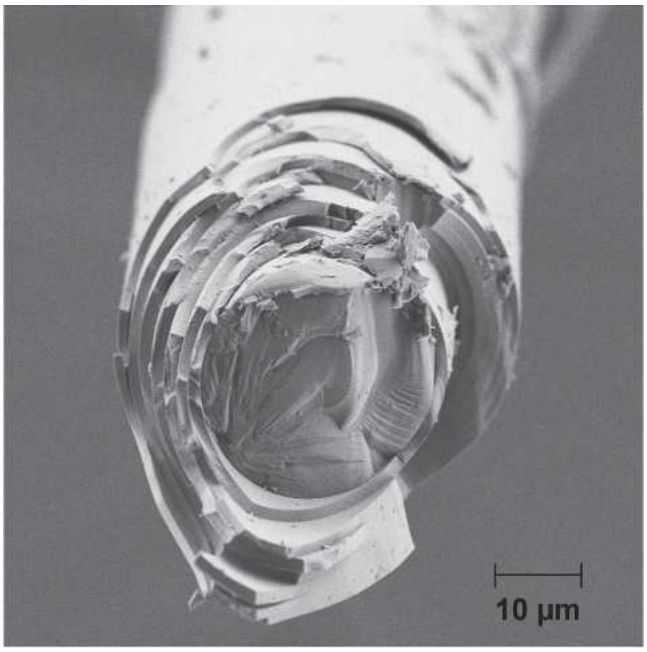


FIG. 2. SEM image of a spicule of *Euplectella aspergillum*, fixed in a droplet of glue, broken and sputtered with palladium. The solid central portion and the layered construction of the outer region are clearly visible.

Several sections from the anchor spicule of one *Monorhaphis chuni* sponge as well as 5 mm × 1 cm portions of the skeletal lattices of four specimens of *Euplectella aspergillum* were embedded in M-Bond AE-15 (M-Line, Raleigh, NC) epoxy. The samples were then sliced into 3-mm-thick sections using a diamond cutting wheel and polished using diamond lapping films down to 0.1-μm grit size under a constant flow of fresh water. A bundle of anchor spicules of *E. aspergillum* was embedded in polymethyl methacrylate (PMMA; Merck KGaA, Darmstadt, Germany), cut with a diamond circular saw, ground with silicon carbide sandpapers, and polished with diamond paste down to a particle size of 1 μm.

Images of all embedded samples were taken with the backscattering detector of an environmental scanning electron microscope (Quanta 600 FEG, FE-ESEM, FEI

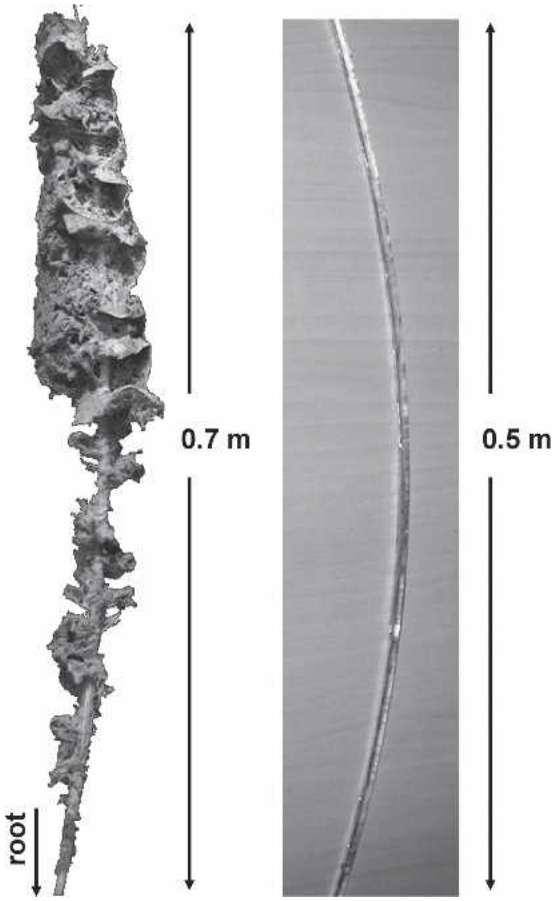


FIG. 3. *Monorhaphis chuni*, photographs of an intact specimen[11] (left) and of a portion of the giant anchor spicule (right).

Germany GmbH, Kassel, Germany) at 30 kV in low vacuum mode (in the following named ESEM). Moreover, images of 10 anchor spicules of *E. aspergillum*, fixed in a small droplet of glue, broken by bending with tweezers, and sputtered with palladium were taken using the secondary electron detector in a scanning electron microscope (Omega 912, Carl Zeiss AG, Oberkochen, Germany) to qualitatively visualize the fracture behavior. Similar analyses were performed with embedded and polished sections of the *M. chuni* spicule. The samples were placed in a small vacuum compatible vice and examined by scanning electron microscopy (SEM; while still in the vice). Because it was a manual vice, there was no possibility to quantify the amount of load placed on the sample. Four different samples were prepared, and 4–6 different areas of each sample were examined.

Additional 25 nonembedded portions of each of the four *E. aspergillum* skeletal lattices were soaked for 10 min in 5 M $NH_4F$:2.5 M HF to visualize the layered structure. The remaining skeletal material was removed, rinsed with de-ionized water and 95% ethanol, dried at 37 °C overnight, and examined with a Tescan Vega TS 5130MM (Czech Republic) thermionic emission SEM.

The embedded giant anchor spicule of *M. chuni* and two anchor spicules of *E. aspergillum* were investigated using a Raman system (WITec, Ulm, Germany). For Raman microspectroscopy, a continuous laser beam was focused on the sample through a microscope. Compositional and crystallographic characteristics of the samples were deduced from peak intensities and bandwidths in the recorded spectra. Compositional properties were quantified using a confocal Raman microscope (CRM200, WITec) with diode pumped green laser excitation (532 nm). The embedded samples were placed on the stage of the microscope and the transverse cross section was oriented perpendicular to the laser beam incident from a 100× (NA = 0 .9, Nikon) microscope objective. With this objective, the instrument is confocal and probes the material in a depth of approximately 3 μm with a depth resolution of 1 μm. Locations of interest were positioned using a motorized XY stage and an optical camera. The spectra were taken using an air-cooled charge-coupled device (CCD; PI-MAX, Princeton Instruments, Trenton, NJ) behind a grating (600 g $mm^{-1}$) spectrograph (Acton Research Corporation, Acton, MA) with a resolution of 6 $cm^{-1}$. All Raman contrast images were acquired with ~1 μm spatial resolution in a rectangular field of view of 200 × 200 μm (1 for *M. chuni* and 2 for *E. aspergillum*) or 200 × 20 μm (3 for *M. chuni* and 2 for *E. aspergillum*) in steps of 1 μm width. Detector integration time for each pixel was 2 s. Images were created by means of the motorized translation stage and reconstruction of pixels.

SAXS[12,13] examinations of two anchor spicules of *E. aspergillum* were carried out using a NanoSTAR diffractometer (Bruker AXS GmbH, Karlsruhe, Germany) with a Cu $K_\alpha$ x-ray source and two crossed Goebel mirrors resulting in a wavelength of $\lambda = 0.154$ nm. The Bruker Hi-STAR area detector was mounted at a distance from the sample of 1050 mm, giving a detectable angular region of up to 2.8°. The freestanding spicules (~50 μm diameter) were placed in the middle of the beam (~200 μm diameter) and measured 2 times for 5 h. Evaluation was done by integration of the intensity in 4 areas per measurement. The area was defined by a scattering angle $2\Theta$ between 0.5 and 2.8 and an azimuthal angle $\Psi$ of 15–75°, 105–165°, 195–255°, and 285–345°. Several measurements were taken from each specimen and averaged as they did not show any significant differences. The intensity was determined as a function of the scattering vector, $q = (4\pi/\lambda) \sin \Theta$, and corrected for background and dark current, using the measured x-ray transmission of the sample, $t = 0.962$. For comparison, a splinter of quartz glass (Heraeus Quarzglas, Heraeus, Hanau, Germany) was measured and evaluated equally ($t = 0.527$).

The mechanical properties of the embedded spicule of *M. chuni* and lattices of *E. aspergillum* and of technical quartz glass were assessed with a Triboscan nanohardness

tester (Hysitron, Minneapolis, MN). In the case of *M. chuni* spicules, nanoindentation was performed with the same specimen used for Raman imaging; however, a different region for examination was chosen to avoid possible artifacts due to surface damage by either technique. Both two line scan (500 indents on *M. chuni* each) and arrays of indents [two times 10 × 10 for two technical quartz glasses with different OH content, 20 × 20 indents and more for the sponge silica (once for *M. chuni* and four times for four specimens of *E. aspergillum*)] were performed with a maximum force of 3000 μN and a distance between the single indents of 5 μm for the line scan and 3 μm for the arrays. This force resulted in an average indent size of about 1 μm and a corresponding indentation depth (contact depth) of 152 ± 8 nm in the sponge silica. Evaluation of the force–displacement curves was performed using the software implemented in the Triboscan, which uses the method proposed by Oliver and Pharr.[14] Although the material tested is a composite of organic material and silica, the Oliver–Pharr method seems applicable due to the small-volume fraction of organic matter. The initial unloading stiffness $S$ is related to the reduced modulus $E_r$ by $S = dP/dH = (2\beta/\sqrt{\pi}) E_r\sqrt{A}$, where $A$ is the projected area of contact and β is an empirical factor to distinguish different indenter shapes (1.034 for Berkovich tip). The reduced modulus accounts for effects of non-rigid indenters, through the equation $1/E_r = (1 - \nu_s^2)/E_s + (1 - \nu_i^2)/E_i$, where $E_s$ and $\nu_s$ are Young's modulus and Poisson's ratio for the sample, and $E_i$ and $\nu_i$ are the indenter's modulus and Poisson's ratio. Statistical evaluation to compare two populations of indents was performed with the t-test implemented in Sigma Plot (SPSS Inc., Chicago, IL).

## III. RESULTS

The investigation of the polished surfaces of the embedded samples from both species, the giant spicule of *M. chuni* and the skeletal spicules of *E. aspergillum,* with ESEM revealed that it was possible to visualize the organic interlayers without etching, although it needed, at least for the latter, very careful adjustments to contrast and brightness, and even under perfect conditions they were not easily detectable (Fig. 4). More important for the evaluation of nanoindentation data from *E. aspergillum* is the distinction between the original spicules and the extra layers of silica cementing them together, which was clearly visible (the arrows in Fig. 4.). The thickness of the silica layers is typically less than 1 μm in *E. aspergillum* and ranges between 1 and 10 μm in *M. chuni*.

Fracture experiments of the anchor spicules of *E. aspergillum* and *M. chuni* were performed as described in Sec. II. Evaluation was performed qualitatively by SEM and clearly revealed the crack path deflection function of

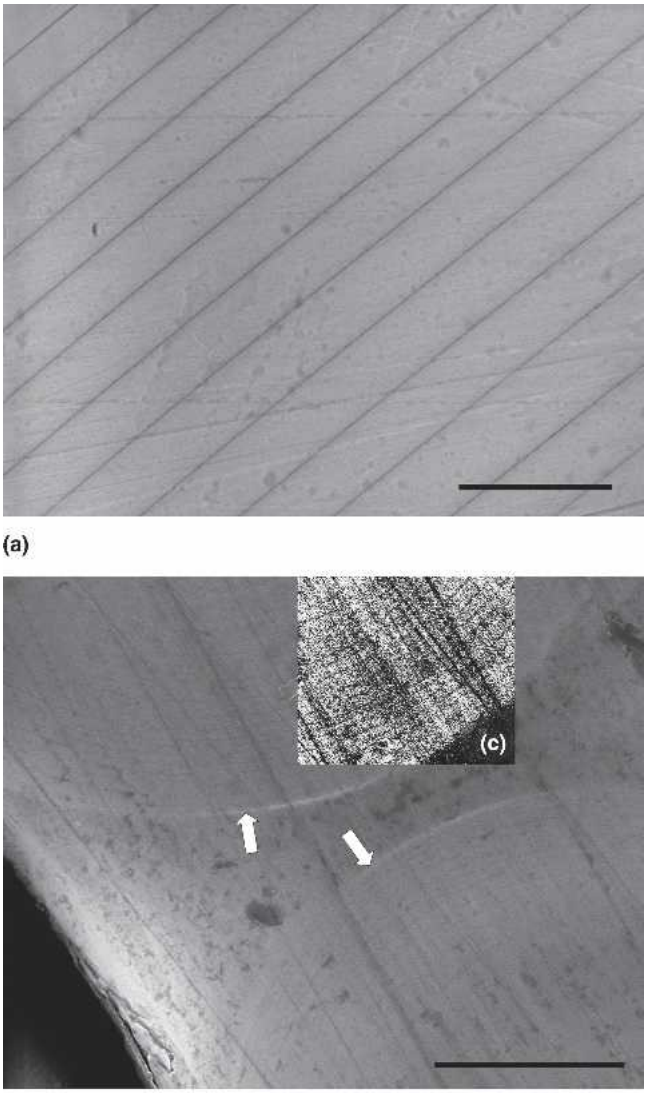


FIG. 4. ESEM images of (a) the embedded, cut, ground, and polished surface of the giant spicule of *M. chuni* and (b) two skeletal spicules of *E. aspergillum*, connected by additional layers of silica cement. The contrast is due to electron density and clearly reveals the organic layers (a). The arrows in (b) indicate the boundaries between spicule and cement. Inset (c) is a region of the image with increased contrast, which then reveals the organic layers having a much smaller spacing than in (a). The length of the scale bars in (a) and (b) corresponds to 10 μm.

the organic interlayers within both species. The *E. aspergillum* samples all showed an irregular fracture surface as visible in Fig. 2, and the sectioned, polished, and compressed *M. chuni* samples all exhibited the distinctive stair-step fracture mode, which can be seen in Fig. 5. There was no variation detected here except that occasionally a few silica layers would fracture together. What varied were the degree of crack opening and the distance of lateral travel along the organic interface between successive cracks which seemed to increase with the applied

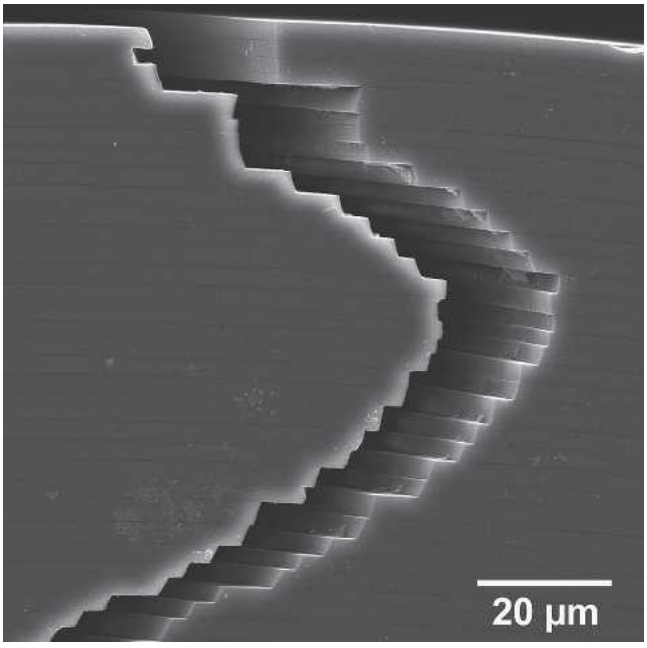


FIG. 5. Fractured anchor spicule of *M. chuni*. The deflections of the crack path from the original direction cause consumption of energy and, therefore, increase the fracture toughness of the spicule.

load, although as mentioned, this was not directly quantifiable.

The small angle x-ray scattering intensity from a single spicule of *E. aspergillum* is shown in Fig. 6. There is a streaklike intensity at small angles, which is due to internal surfaces, probably the interfaces between silica and the organic interlayers. In addition, there is a diffuse intensity at somewhat larger angles that reveals particles of very small dimensions. A Guinier plot[12] shows a well-defined linear region, which can be used to fit the size of the nanoparticles which produce this scattering, using the Guinier approximation $I(q) \propto \exp(-R^2q^2/5)$, where $R$ is the particle radius. The analysis (Fig. 6) shows that the diameter of the particles is approximately 2.8 nm. In contrast to this, SAXS from a technical glass did not show any comparable signal (Fig. 6). There is no direct evidence for the nature of the particles seen in SAXS, but given the small amount of protein present in the spicule, the signal is most likely due to silica and indicates that the silica matrix is built from small colloids with a diameter in the order of 2.8 nm. This size is much smaller than the 50–200 nm diameter of spheres revealed by etching[5] (Fig. 7). In fact, SAXS is not even sensitive to structures with dimensions larger than 50 nm. It is, therefore, very likely that the spheres visible in Fig. 7 have a substructure and are composed themselves of silica colloids in the size range below 3 nm.

Further analysis of the two-dimensional SAXS signal shows that it is perfectly isotropic, which might indicate that the particles do not have a long-range order (such as

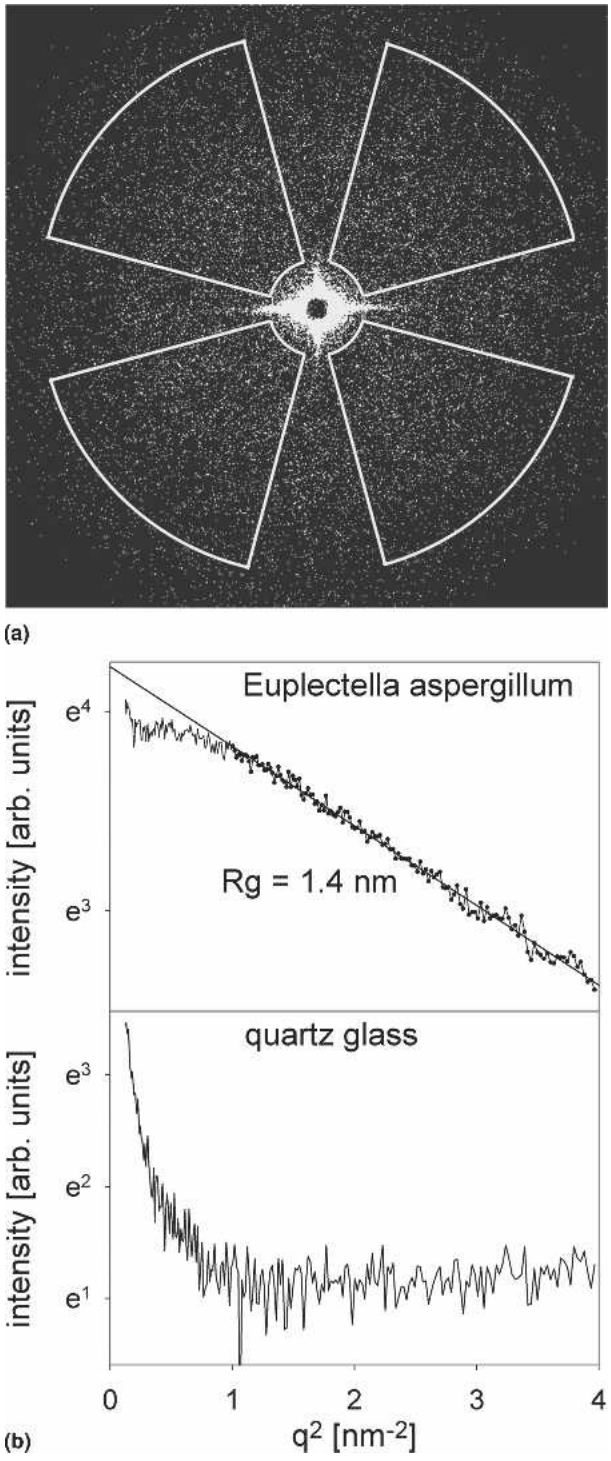


FIG. 6. SAXS investigation of a vertically oriented single anchor spicule of *E. aspergillum*. The two-dimensional SAXS pattern is shown on the left. The streaks next to the beam stop are due to the internal interfaces (probably the organic interlayers). In addition, there is a diffuse intensity, which reveals nano-sized particles. The white lines border the area within which the integration used for evaluation took place. The right side shows Guinier plots [that is, log (intensity) versus $q^2$] of the radially integrated SAXS intensity for a spicule (a) and commercial quartz glass (b). The slope of the graph in the linear regime gives a sphere radius of about 1.4 nm for the nanoparticles.

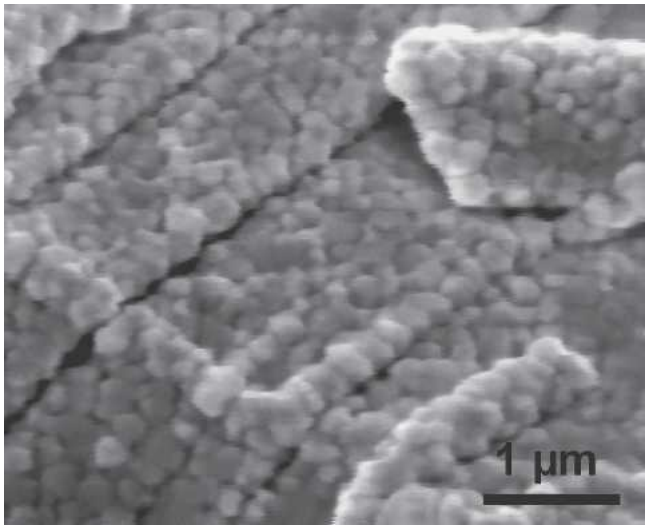


FIG. 7. Scanning electron microscopic image of an etched spicule cross-section from *Euplectella aspergillum*, revealing its colloidal structure. The size of the particles ranges from 50 to 200 nm and is much larger than those revealed by SAXS.

a near crystalline arrangement). There is, however, a deviation from the straight line at small $q$-values, which indicates the existence of a weak short-range order (average spacing) between the particles.[12,13]

Raman spectroscopic imaging was used to visualize the organic interlayers in *M. chuni* (Fig. 8). These organic interlayers clearly show strong amide vibrations (1655 $cm^{-1}$), confirming that they contain protein.[15,16] Similar images could not be obtained for *E. aspergillum* because the spatial resolution of the Raman system was about 1 μm, which is larger than the spacing between organic layers in these spicules, but the existence of amide vibrations could also be confirmed there. In addition, C–H vibrations (2937 $cm^{-1}$) were detected not only in the organic interlayers, but also in a region of ~30-μm diameter around the central organic filament, proving that there is an increased amount of organic matter in this region. In the same central region, an increased OH content of silica was also revealed by the ratio between the intensities of Si–O–Si (about 800 $cm^{-1}$) and silanol (975 $cm^{-1}$) vibrations.[17] It is noteworthy that in this region, which has a high refractive index due to an increased sodium content,[18,19] there is also an increased content of organic matter and a comparatively high degree of hydration.

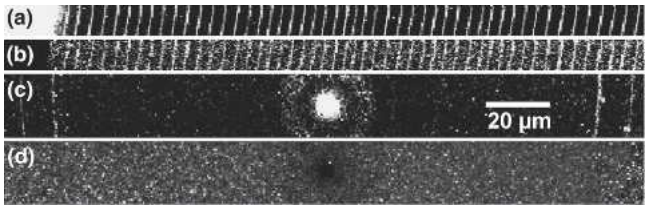


FIG. 8. Raman images of spicule cross-sections from *Monorhaphis chuni*: (a) C–H stretch vibration and (b) amide vibration in the periphery of the spicule (embedding medium is visible on the far left side); (c) C–H stretch vibration and (d) ratio between intensity of Si–O–Si and Si–O–H vibrations in the central region of the spicule. The central filament is clearly visible with a halo of organic matter around it (c).

Nanoindentation was used to assess the mechanical properties of the spicule material in *M. chuni* and *E. aspergillum*. The layer thickness of silica in *M. chuni* (~6 μm, compare Fig. 4) enables one to distinguish between indents hitting the organic interlayer and indents between them, a distinction that is not possible in *E. aspergillum*, due to the size limitations. As a consequence, only average values of mechanical properties for the silica–protein composite could be determined for *E. aspergillum,* while a detailed profile within individual lamellae could be obtained for *M. chuni.*

First, line scans across the entire cross section of the *M. chuni* spicule were performed. The maximum indentation force of 3000 μN resulted in an indent of about 1 μm in width and 0.15 μm in depth (according to the geometry of Berkovich indenter tip, tetrahedral shape with a side to edge inner angle of 142.35°).

Statistical evaluation for the line scan shown in Fig. 9 revealed no significant difference in hardness ($p = 0.89$) but a significant difference in the reduced modulus ($p = 0.011$) between the non-layered central and the layered peripheral region of the *M. chuni* spicule (regions c and b in Fig. 9).

In a second experiment, an array of indents on the *M. chuni* spicule cross section was set with the same maximum force of 3000 μN and a distance between the

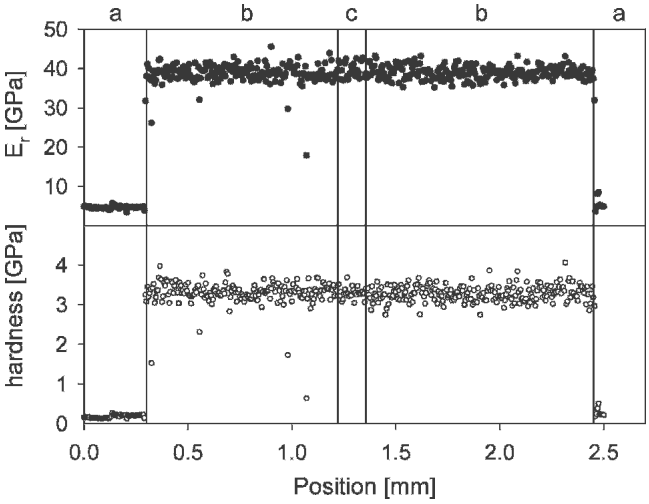


FIG. 9. Evaluation of a line scan of nanoindents performed across the cross section of a giant spicule of *M. chuni*. Reduced modulus and hardness are plotted as function of position, in (a) the embedding medium, (b) the periphery, and (c) the central region. The central region corresponds to the area without organic interlayers shown in Fig. 8(c). No distinction was made between indents hitting an organic interlayer or silica only.

indents of 3 μm. The position of the array was about 350 μm off the center axis of the spicule. Results for the reduced modulus are shown in Fig. 10.

Indents were assigned to two different regions: the vicinity of the interlayers and the bulk of the silica layers. The results for each silica layer and the corresponding interlayer region as a function of the distance from the center of the spicule are shown in Fig. 11. Material close to interlayers was significantly more compliant ($p$ = 0.0001) and softer ($p < 10^{-9}$) than material far from the interlayers in the *M. chuni* spicule.

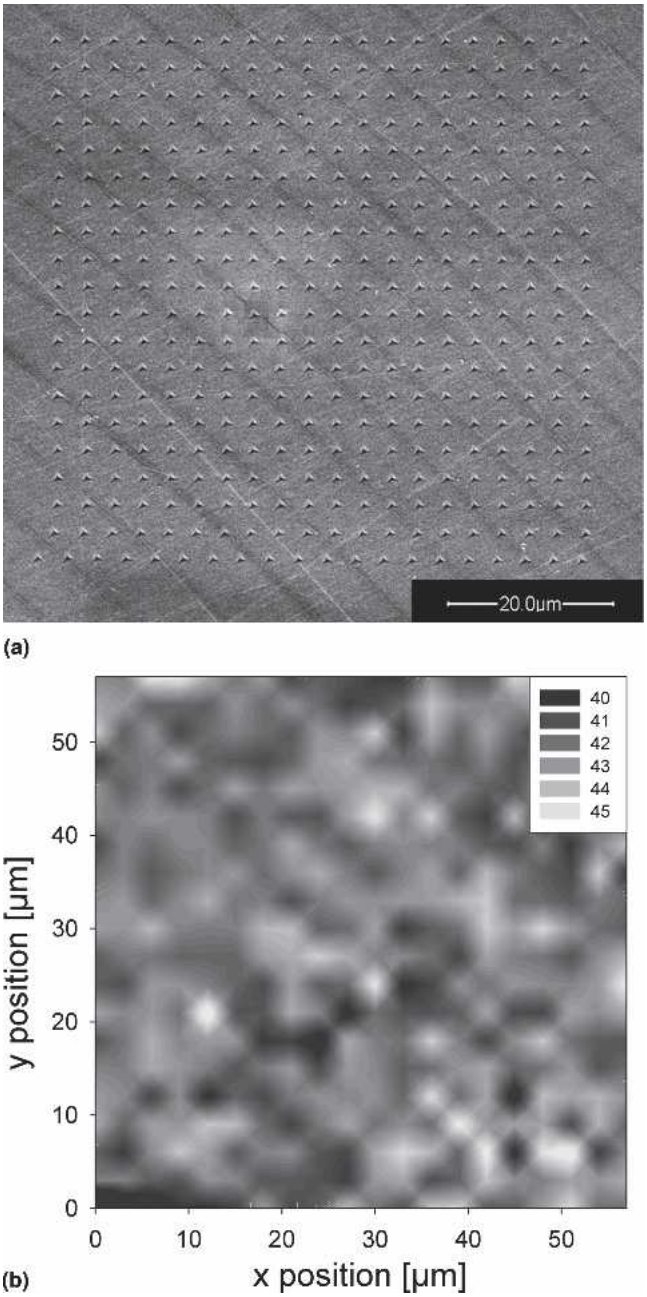


FIG. 10. (a) ESEM image of the array of indents and (b) contour plot of the reduced modulus in a spicule cross-section of *M. chuni*. The dark lines in the ESEM image (using the back-scattering detector) are the organic interlayers.

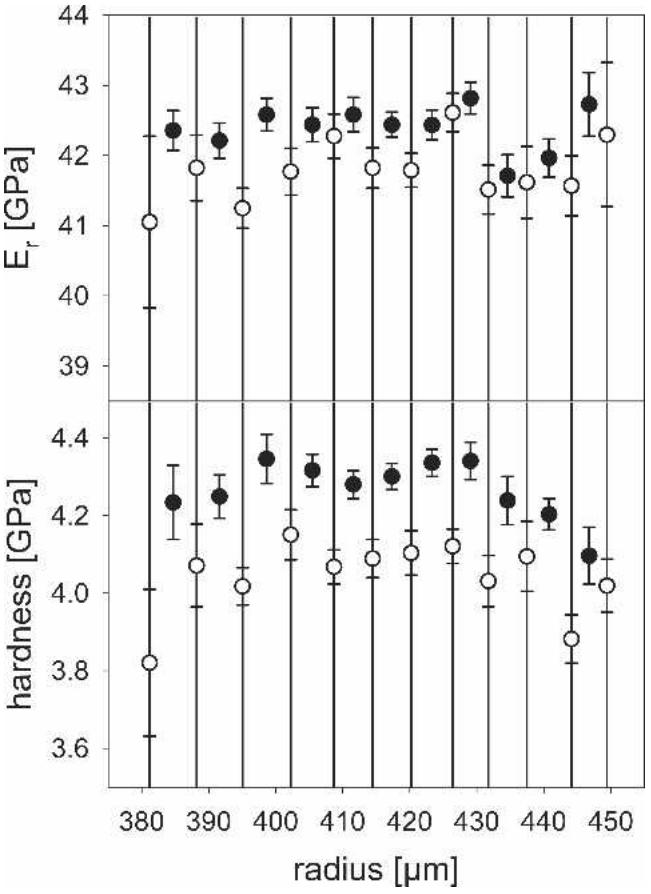


FIG. 11. Averaged values of reduced modulus (upper part) and hardness (lower part) of the indents within each silica layer as a function of the distance from the center of a *M. chuni* spicule (radius). Indents touching the organic interlayer (open symbols) and away from the interlayer (full symbols) are analyzed separately. The gray vertical lines show the positions of the organic interlayers.

A more detailed analysis is shown in Fig. 12. For each indent, the distance to the closest organic interlayer was measured. All the indents with a given distance (within ±0.125 μm) to the closest interlayer were pooled, and the reduced modulus and hardness were averaged.

Figure 12 shows an interesting graduation of the properties within each silica layer. Typically the layer appears softer close to the organic interlayer. It is not clear, however, whether this reflects an inherent gradation of the silica properties or just the fact that the response to mechanical load is somewhat different due to the proximity of an organic interlayer.

In a further set of experiments, four arrays of indents were set on the embedded skeletal lattices of *E. aspergillum*. Due to the small thickness of the silica layers (less than the size of the indentation), it was not possible to determine any intra-lamellar variations in the properties. The aim here was to assess whether there are

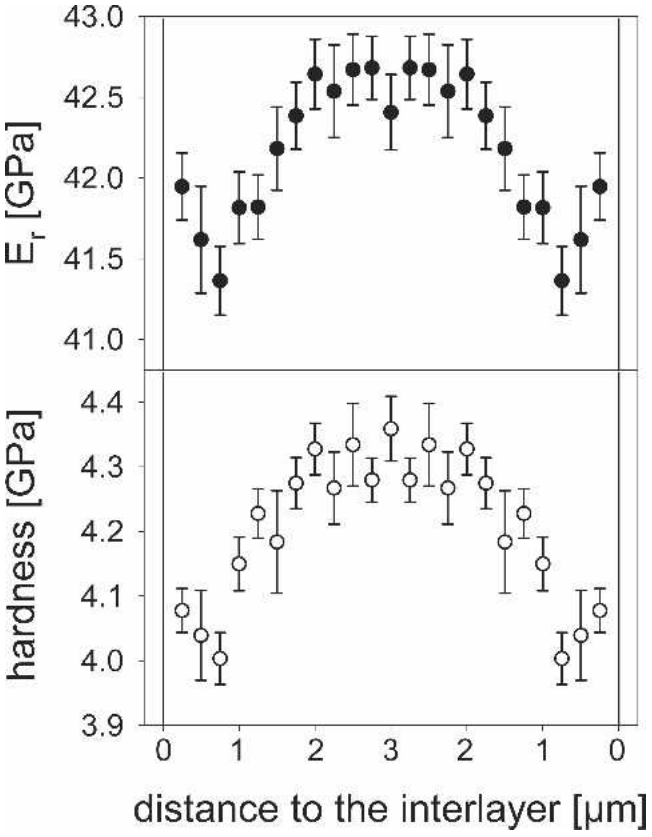


FIG. 12. Average reduced modulus (upper plot) and hardness (lower plot) as a function of the distance to the closest organic interlayer in *M. chuni*. All data points with a distance between $0.25n - 0.125$ and $+ 0.125$ μm ($n$ being an integer) were pooled and the average value plotted at the position $0.25n$ μm. The data have been mirrored around the center of the silica layer (at position 3 μm). Again, the gray vertical lines show the positions of the organic interlayers.

differences in the mechanical properties of the spicules compared to the silica cement that joins them together. In the maps of the mechanical properties [Fig. 13(b)], differences between the two regions are not immediately obvious, but a more detailed analysis by assignment of the indents to certain regions, either the spicule region or interspicular cement [Fig. 13 (c)], and statistical evaluation revealed a small but highly significant difference between them for each of the indent arrays. The reduced modulus and hardness were 34.4 ± 1.3 GPa and 2.86 ± 0.20 GPa (mean ± standard deviation) and 35.2 ± 1.1 GPa and 3.07 ± 0.1 GPa, for regions 1 and 2, respectively. Both modulus and hardness are significantly different between the regions with $p = 0.01$ and $p < 0.001$.

Finally, commercial quartz glass with different hydration (Heraeus Quarzglas, Heraeus, Hanau, Germany) was tested under similar conditions for comparison. Average values of reduced modulus and hardness are summarized in Fig. 14 for both silica sponge species in comparison to the commercial quartz glass. In this figure, we did not differentiate between the areas of silica close to the

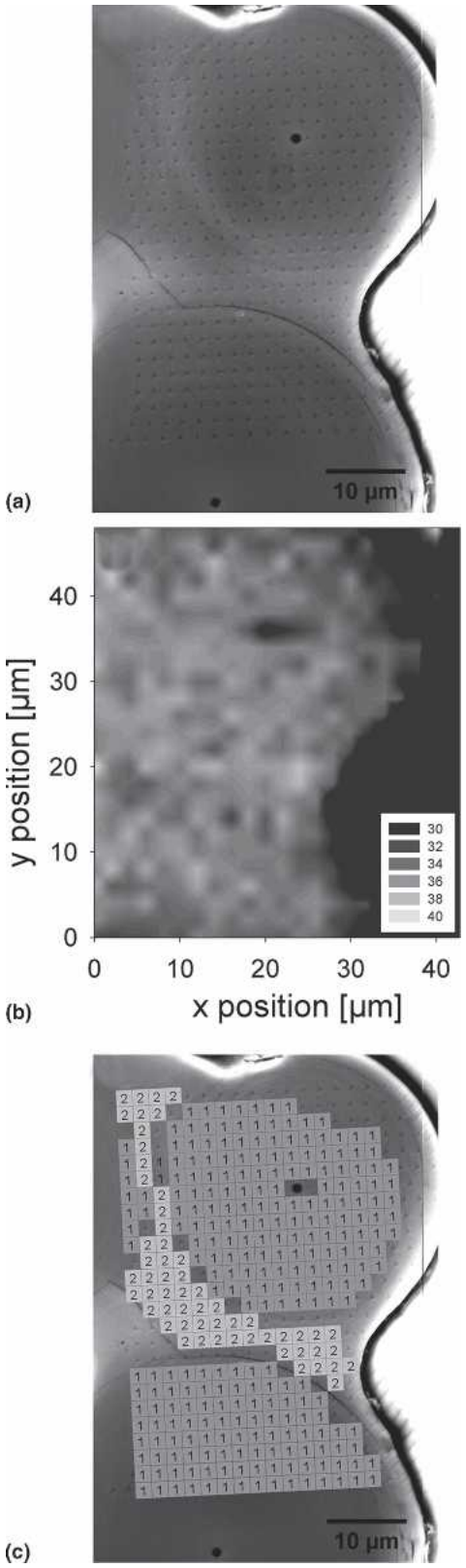


FIG. 13. Micromechanical testing of bundles of spicules from *E. aspergillum*: (a) array of indents visualized by backscattered electron imaging, (b) reduced modulus map from nanoindentation, and (c) assignment of the indents to different regions (1 = spicule, 2 = cement).

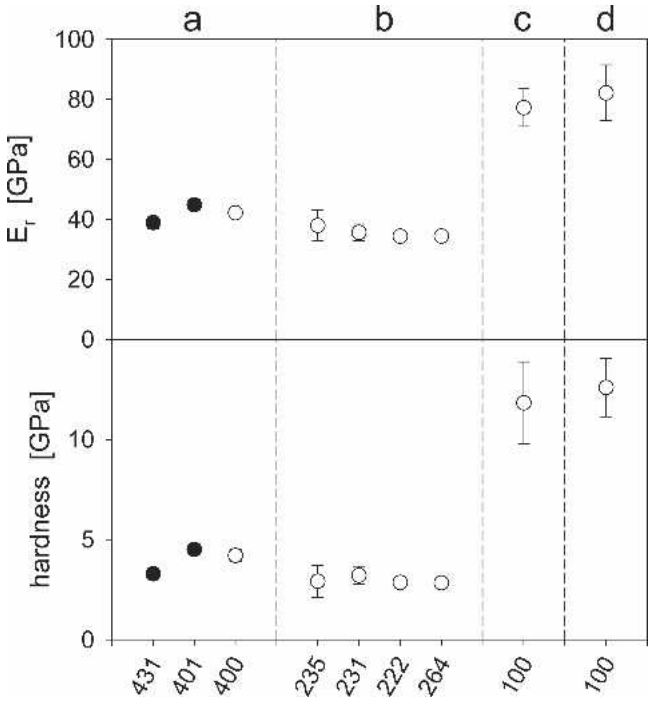


FIG. 14. Summary of the nanoindentation experiments for (a) spicules of *M. chuni*, (b) spicules of *E. aspergillum*, and technical quartz glass with (c) low and (d) high $OH^-$ content. Average reduced modulus ($E_r$) and hardness are plotted with error bars representing standard deviations. The numbers on the abscissa correspond to the quantity of indents used for each evaluation. Closed symbols indicate line scans and open symbols area scans.

organic interlayers and far away from them in *M. chuni* because this distinction was not possible in *E. aspergillum*. Figure 14 shows that technical quartz glass has a reduced modulus and hardness about two times higher than the values obtained for biological silica, in accordance with Refs. 9 and 20.

## IV. DISCUSSION

In our experiments, we showed that the spicules of *E. aspergillum* are composites on three levels of hierarchy. On the nanometer scale, we found silica nanospheres in a silica matrix on two different orders of magnitude. SAXS, on the one hand, gives evidence for nanospheres with a diameter of ~3 nm. Etching and high-resolution SEM, on the other, reveal much larger spheres with a diameter between 50 and 200 nm. Most likely, these larger spheres are formed by an agglomeration of the smaller ones. Additionally, the spicules have a layered composition on the micrometer scale, which can be visualized by ESEM or Raman spectroscopy. In the ESEM images, the organic interlayers are darker because of a lower electron density. This is also valid for the vicinity of the axial filament, a finding which is in accordance with the results of the Raman investigation. Additionally, the clear visibility of amide and C–H vibrations at the interfacial regions proves that the organic interlayers contain protein. As opposed to members of the other class of siliceous sponges, the demospongiae, the spicule-associated proteins of hexactinellids have yet to be fully sequenced. Moreover, the degree of interrelatedness of the various sponge classes remains to be unambiguously resolved.[21] Thus, it is not possible for the time being to tell which proteins are the source of the amide and C–H vibrations detected in *E. aspergillum* and *M. chuni*.

The stiffness of the sponge silica is about half the stiffness of technical quartz glass, a finding which is in accordance with the results of tensile tests in Ref. 10. It could result from the composition of silica nanospheres in a silica matrix and from different chemical composition, especially a high content of organic matter and OH groups. Furthermore, experiments by Levi et al.[20] on anchor spicules of *M. chuni* and Sarikaya et al.[9] on spicules of *Rossella racovitzae*, another hexactinellid, have shown in three point bending tests that the strength of the sponge silica is at least three times the strength of technical silica. Combining this with the much lower stiffness, it is most likely that the sponge silica is much more deformable and, hence, much less brittle than technical glass.

As silica is a brittle material, its strength is determined by the largest present cracks (Weibull statistics[22]), which start to grow as soon as the critical stress is reached. The increase in strength in the sponge silica is most likely due to an effective crack stop or deviation mechanism, which neutralizes large cracks. Part of this could be an effect at the nanoscale due to the colloidal structure of biosilica. However, crack deviation definitely occurs at the micrometer scale, at the organic interlayers, as shown in Fig. 5. The crack patterns are fully consistent with those previously found in spicules of a different species of the class Hexactinellida, *Rossella racovitzae,*[9] although in this study we did not analyze fracture toughness quantitatively.

It is not clear whether the gradient of the mechanical properties of the silica from the vicinity of the organic interlayer to the region further away from it (see Fig. 12) plays a role for the mechanical properties of the overall material. The differences are small and could result from edge effects in the indentation process, where indents close to the organic interlayer find mechanical boundary conditions different from those of the material further away from it. It is interesting though, that the gradient of stiffness and hardness depicted in Fig. 12 is mirrored by the etching process, which seems to attack the silica close to the organic interlayers more easily than the silica further away from the interlayers (see Fig. 15). Moreover, the refractive index is known to vary in a similar manner inside each layer.[18] This supports the idea that

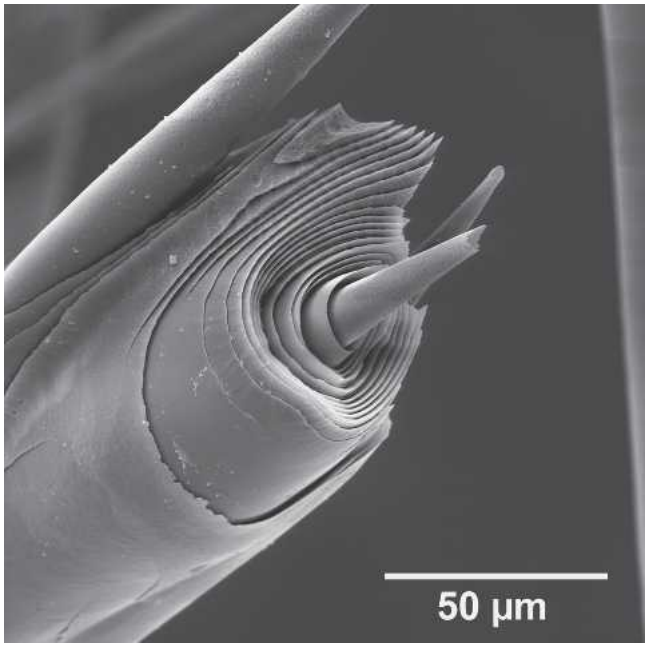


FIG. 15. SEM image showing a spicule of *E. aspergillum* that was etched in HF.

the variation in stiffness is due to a varying composition rather then just edge effects. As opposed to other biological materials like bone and dentin, there is almost no gradient in the degree of mineralization of the sponge silica. Bone and dentin are composite materials consisting of mineral and organic components intimately associated with one another on the nanometer scale whereas the sponge spicules are essentially a macro-composite, as the silica layers between the organic interlayers contain no detectable quantities of organic material. Apart from the organic interlayers and the vicinity of the axial filament, the brightness in the ESEM images is relatively constant, indicating a constant mineral density. Furthermore, the growth and maturation mechanism of these sponge spicules differs greatly from what is observed in materials like bone.[23] There is no evidence for replacement of old, damaged material by new material, which is then successively mineralized. The only distinction that can be made in sponges (as far as age is concerned) is between the original spicules and the cement, which is deposited later.[3] Even there, the volume fraction of organic matter, representing a degree of mineralization, is very similar to that of the underlying spicules.

It is certain that the presence of organic interlayers is not only deviating cracks but lowers the overall stiffness and hardness of the composite, as compared to biosilica without organic interlayers. This influence of organic interlayers could perhaps explain why the spicules of *E. aspergillum* have lower stiffness and hardness than the anchor spicule of *M. chuni* because they have a higher density of organic interlayers. Similarly, the difference between the spicules and the cement in *E. aspergillum* might just result from the slightly lower density of organic interlayers in the cement. However, such an effect could never explain the much higher stiffness of technical quartz glass. The composition of the biosilica itself must be responsible for this. This finding is consistent with the stiffness values reported for *Rossella racovitzae* to be lower than those of technical glass, which was attributed to a higher water content of the sponge silica.[9] Interestingly, the scattering of nanoindentation data from different sections (Fig. 14) seems to be quite larger than the deviations within a given section [as measured by line scans (Fig. 9) or by area scans (Fig. 13)]. We do not have a definitive answer as to where this difference between sections originates, though it might be partially due to natural variations within different specimens or between macroscopic locations of the giant spicule.

It is noteworthy that most of the significant findings discussed here were made possible only because of the use of the giant anchor spicule of *M. chuni*. No other described species of sponge synthesize spicules are even remotely comparable in dimensions to that encountered in this species. This attribute makes it an ideal research subject for mechanical and compositional studies of biosilica, using techniques that are dimensionally limited in spatial resolution. Such studies are critical for understanding the structural and mechanical properties of biological materials that show advantageous design features, and the present work is yet another example of a detailed nano- and micromechanical characterization of such materials.

## ACKNOWLEDGMENTS

We thank B. Richer de Forges, IRD, Nouméa, New Caledonia, for collecting the giant spicules of *M. chuni* and Michael Porter, Amy Butros, Youli Li, David Kisailus, and Birgit Schwenzer for their help and discussions. James Weaver and Daniel Morse were supported by grants from the NOAA National Sea Grant College Program, U.S. Department of Commerce (NA36RG0537, Project R/MP-92) through the California Sea Grant College System, NASA (NAG1-01-003 and NCC-1-02037), and the Institute for Collaborative Biotechnologies through Grant No. DAAD19-03D-0004 from the Army Research Office.

## REFERENCES

1. J.G. Gehling and J.K. Rigby: Long expected sponges from the neoproterozoic ediacara fauna of South Australia. *J. Paleontol.* **70**(2), 185 (1996).
2. M. Brasier, O. Green, and G. Shields: Ediacarian sponge spicule clusters from southwestern Mongolia and the origin of the Cambrian fauna. *Geology* **25,** (1997).

3. T. Saito, I. Uchida, and M. Takeda: Skeletal growth of the deep-sea hexactinellid sponge *Euplectella oweni,* and host selection by the symbiotic shrimp *Spongicola japonica* (Crustacea: Decapoda: Spongicolidae). *J. Zool.* **258,** 521 (2002).
4. M. Berggren: Spongiocaris hexactinellicola, a new species of stenopodidean shrimp (Decapoda, Stenopodidae) associated with hexactinellid sponges from Tartar Bank, Bahamas. *J. Crustacean Biol.* **13,** 784 (1993).
5. J. Aizenberg, J.C. Weaver, M.S. Thanawala, V.C. Sundar, D.E. Morse, and P. Fratzl: Skeleton of *Euplectella sp*.: Structural hierarchy from the nanoscale to the macroscale. *Science* **309,** 275 (2005).
6. J.C. Weaver and D.E. Morse: Molecular biology of demosponge axial filaments and their roles in biosilicification. *Microsc. Res. Tech.* **62,** 356 (2003).
7. G. Mayer: Rigid biological systems as models for synthetic composites. *Science* **310**(5751), 1144 (2005).
8. C.C. Perry and T. Keeling-Tucker: Biosilicification: The role of the organic matrix in structure control. *J. Biol. Inorg. Chem.* **5,** 537 (2000).
9. M. Sarikaya, H. Fong, N. Sunderland, B.D. Flinn, G. Mayer, A. Mescher, and E. Gaino: Biomimetic model of a sponge-spicular optical fiber—Mechanical properties and structure. *J. Mater. Res.* **16**(5), 1420 (2001).
10. S.L. Walter, B.D. Flinn and G. Mayer: Mechanisms of toughening of a natural rigid composite. *Mater. Sci. Eng., C* (2005, in press).
11. F.E. Schulze: *Hexactinellida*, in *Scientific Results of the German Deep-Sea Expedition with the Steamboat, "Valdivia" 1898-1899,* edited by C. Chun (Verlag Gustav Fischer, Jena, Germany, 1904).
12. A. Guinier and G. Fournet: *Small-Single Scattering of X-rays* (Wiley, New York, 1955).
13. P. Fratzl: Small-angle scattering in materials science—A short review of applications in alloys, ceramics and composite materials. *J. Appl. Crystallogr.* **36,** 397 (2003).
14. W.C. Oliver and G.M. Pharr: An improved technique for determining hardness and elastic-modulus using load and displacement sensing indentation experiments. *J. Mater. Res.* **7,** 1564 (1992).
15. J.T. Pelton and L.R. McLean: Spectroscopic methods for analysis of protein secondary structure. *Anal. Biochem.* **277**(2), 167 (2000).
16. O. de Carmejane, M.D. Morris, M.K. Davis, L. Stixrude, M. Tecklenburg, R.M. Rajachar, and D.H. Kohn: Bone chemical structure response to mechanical stress studied by high pressure Raman spectroscopy. *Calcif. Tissue Int.* **76**(3), 207 (2005).
17. E. Gailliez-Degremont, M. Bacquet, J. Laureyns, and M. Morcellet: Polyamines adsorbed onto silica gel: A Raman microprobe analysis. *J. Appl. Polym. Sci.* **65,** 871 (1997).
18. J. Aizenberg, V.C. Sundar, A.D. Yablon, J.C. Weaver, and G. Chen: Biological glass fibers: Correlation between optical and structural properties. *Proc. Natl. Acad. Sci. USA* **101,** 3358 (2004).
19. V.C. Sundar, A.D. Yablon, J.L. Grazul, M. Ilan, and J. Aizenberg: Fibre-optical features of a glass sponge—Some superior technological secrets have come to light from a deep-sea organism. *Nature* **424,** 899 (2003).
20. C. Levi, J.L. Barton, C. Guillemet, E. Lebras, and P. Lehuede: A remarkably strong natural glassy rod—The anchoring spicule of the *Monorhaphis* sponge. *J. Mater. Sci. Lett.* **8,** 337 (1989).
21. A. Rokas, D. Kruger, and S.B. Carroll: Animal evolution and the molecular signature of radiations compressed in time. *Science* **310,** 1933 (2005).
22. W. Weibull: A statistical distribution function of wide applicability. *J. Appl. Mech. Trans. ASME* **18**(3), 293 (1951).
23. P. Fratzl, H.S. Gupta, E.P. Paschalis, and P. Roschger: Structure and mechanical quality of the collagen-mineral nano-composite in bone. *J. Mater. Chem.* **14,** 2115 (2004).